Research Square

Preprints are preliminary reports that have not undergone peer review.
They should not be considered conclusive, used to inform clinical practice,
or referenced by the media as validated information.

Interfacial Bond Strength of Concrete-Filled Galvanized Steel Tubes: Push-Out Experiments, Geometry-Grouped Machine Learning, and Multi-Criteria Optimization

Chethan Kumar S
Jakson Green Limited
Sandesh N U
apsarpasssha1982@gmail.com
B.M.S College of engineering
T S Anusha
Jakson Green Limited
N. S. Kumar
Ghousia College of Engineering
L K Ashwini
Dr Ambedkar Institute of Technology
Syed Sharfuddin
Ghousia College of Engineering
Apsar Pasha
Ghousia College of Engineering

Research Article

Keywords: concrete-filled steel tube, galvanized steel tube, interfacial bond, push-out test, Taguchi design, support vector regression, MOORA, COPRAS

Posted Date: September 17th, 2026

DOI: https://doi.org/10.21203/rs.3.rs-10688604/v1

License: This work is licensed under a Creative Commons Attribution 4.0 International License.
Read Full License

Additional Declarations: No competing interests reported.

Abstract

Interfacial load transfer governs composite action in concrete-filled steel tubes, yet the combined effects of concrete strength and tube geometry remain difficult to quantify when experiments are limited. This study evaluates the push-out bond strength of concrete-filled galvanized steel tubes using 27 reported observations arranged as three concrete grades (nominal M40, M50, and M70) across a Taguchi L9 geometry matrix comprising tube diameters of 33.7–48.3 mm, wall thicknesses of 2.6-4.0 mm, and length-to-diameter ratios of 12–16. The measured bond strength ranged from 0.830 to 2.062 MPa. Main-effect analysis and analysis of variance identified L/D as the dominant factor (33.13% contribution, $p < 0.001$), followed by wall thickness (19.43%, $p = 0.003$), concrete strength (17.44%, $p = 0.004$), and diameter (8.86%, $p = 0.043$). To avoid optimistic model assessment, machine-learning models were evaluated by nested, geometry-grouped cross-validation, in which all concrete grades sharing one L9 geometry were withheld together. Support vector regression provided the best generalization ($R^2 = 0.719$, RMSE = 0.193 MPa, MAE = 0.157 MPa, and MAPE = 10.87%), whereas tree ensembles were less reliable for this small structured dataset. Entropy-weighted MOORA and COPRAS analyses, together with the Taguchi larger-the-better criterion, consistently selected D = 42.2 mm, t = 4.0 mm, and L/D = 12 as the robust optimum; the corresponding bond strengths were 1.899, 1.915, and 1.802 MPa. The results show that a short, thick-walled tube geometry provides the most stable interfacial resistance within the investigated domain, while grouped validation is essential for credible data-driven prediction from compact experimental designs.

1. Introduction

Concrete-filled steel tubular (CFST) members combine the tensile resistance and ductility of a steel shell with the compressive resistance and stability of an infilled concrete core. Their structural efficiency has led to widespread use in building columns, bridge piers, piles, industrial supports, and other members subjected to high axial demand. The intended composite action, however, depends on the transfer of longitudinal shear across the steel-concrete interface. If this interface slips or debonds, the steel tube and concrete core cannot fully share load, local stress concentrations develop, and the stiffness and resistance assumed in design may not be mobilized. Early work on composite action demonstrated that interfacial shear transfer is therefore a governing aspect of load introduction and force redistribution in concrete-filled tubes [1]. The bond of CFST members is created by chemical bonding, micromechanical bonding, friction, radial pressure, and irregularities of the surfaces at the contact area. These mechanisms are developed when loading. As the adhesion is lost, slip begins and the friction and mechanical interlock take over as the main part of the residual response. The normal pressure and effective contact condition at the interface can be changed due to concrete shrinkage, creep, geometry of the tubes, curing history and confinement. These mechanisms can be isolated by using push-out testing, as the concrete core can move relative to a supported steel tube, allowing full bond-slip response and, if instrumented, the ultimate interfacial resistance to be measured [2–5]. If one material property is proposed as a control, then experimental studies reveal that this is not the case. In this regard, Tao et al. [2] tested several circular and rectangular CFSTs, and highlighted the importance of

section size, interface length, concrete condition and surface preparation. Qu et al. [4] also reported that the response of rectangular CFST can significantly change as a result of load-reversed push-out tests considering interface treatment and cyclic slip history.

There has been a significant effort to enhance the radial contact force and increase the push-out resistance by means of expansive concrete [5] and post-fire and elevated temperature tests have shown that the interfacial mechanism can vary under such circumstances due to differential thermal deformation and degradation of the materials [6, 7]. The use of recycled aggregate concrete, stainless steel tubes, connectors, and the modification of the inner surfaces have also been studied to try to improve or reinterpret bond transfer [8–11]. All of these studies suggest that these geometric variables should not be evaluated separately, but in combination with specific properties. Galvanized steel tubes provide a functional protection from corrosion and are appealing when it comes to exposed lightweight and modular structural systems. The zinc coated interface is however unique from the untreated carbon-steel: it is rougher, harder, less continuous and interacts with the cementitious pore solution which may affect adhesion and friction. A strict interpretation would then call for an explicit report of the surface condition and, preferably, comparison with an ungalvanized sample. The present data set includes only galvanized tubes and so can measure the joint response of both concrete strength and geometry in that system but cannot provide a measure of the galvanizing effect. Compact designs of experiments are useful if the preparation of specimens and fullscale structural testing is costly. A Taguchi orthogonal array is also efficient at distributing various levels of the factors and permits main-effect estimation to be carried out in significantly less number of combinations than does a full factorial program [12]. Several response conditions can be combined using multi criteria decision methods. MOORA is based on vector normalization and differentiates beneficial from non-beneficial criteria [13] while COPRAS considers relative utility based on normalized weighted performance. The entropy weighting gives a data-based index of the discriminatory information content of each response criterion [14]. The methods can be used only if their intended direction and the interpretation of the weights are explicitly defined, otherwise seemingly precise rankings can mask the real experimental trades off. In addition to the conventional approach, machine learning (ML) provides an alternative way to estimate nonlinear relationships between bond strength and the material and/or geometric parameters. Random forests, gradient boosting and support vector regression (SVR) have been increasingly implemented to structural datasets, and recently, other surrogate models, such as artificial neural networks have been tried in CFST studies to predict capacity or interfacial performance [15–17]. Small data sets pose a special risk: flexible models can fit the data that has been used and can produce good looking R-squared values, but they do not generalize to an unseen geometry. Additionally, having the same observations being used for both hyperparameter selection and performance reporting creates selection bias [18]. Random observation level splitting also leaks geometry information between train and test sets in structured experiments when the geometry is the same in multiple concrete grades. The grouping of the experiment should therefore be maintained in the validation.

In this context, the present work revisits a dataset of 27 observations of push-out tests performed on concrete-filled galvanized steel tubes (GFST) in a unified experimental/statistical/predictive approach.

The objectives of this paper are to quantify the influence of concrete strength, tube diameter, thickness of the tube wall and L/D ratio on ultimate interfacial bond strength, compare the regression models by means of nested geometry-grouped validation and find a robust geometry for three concrete strengths by applying Taguchi, entropy-weighted MOORA and COPRAS methods. The principal contribution is not a universal design equation, but a clear small-data flow for going from apparent fit to generalization, from factor effects to prediction to optimization, to the same fixed experimental evidence.

2. Materials and methods

2.1 Concrete and steel-tube variables

The three conventional concrete mixtures were prepared using the procedure for mix-design as reported in IS 10262:2009. The nominal grades were M40, M50 and M70. The quantities of constituents, water-cement ratio, average 28-day cube strengths and moduli of elasticity are summarized in Table 1. 150 mm cubes were used for compressive strength tests as per IS 516. The average strengths measured were 41.60, 51.86 and 72.60 MPa, which is consistent with separation of the three levels of concrete. The nominal values used for the models, 40, 50, and 70 MPa, are kept in the manuscript as inputs to the models for the push-out results reported.

Table 1
Concrete mixture proportions and reported mechanical properties.

Property	M40	M50	M70
Cement (kg/m³)	336	408	445
Fine aggregate (kg/m³)	940	880	860.5
Coarse aggregate (kg/m³)	674	632	617
Water (kg/m³)	168	184	187
Water/cement ratio	0.50	0.45	0.42
Cement:fine:coarse ratio	1:2.8:2.0	1:2.0:1.5	1:1.94:1.38
Average 28-day cube strength (MPa)	41.60	51.86	72.60
Young's modulus (MPa)	21,019	25,743	29,725

The outer diameters of the tubes tested were 33.7, 42.2 and 48.3 mm and the nominal wall thickness was 2.6, 3.2 and 4.0 mm respectively. The coefficient of variation (CV) of these variables ranges from 8.43 to 18.58. The thickness of the zinc coat, the type of steel, yield strength, ultimate tensile strength, elastic modulus and surface roughness of the internal surfaces were not provided in the experimental record supplied, and should be entered prior to submission as these parameters have an impact on the reproducibility and mechanics of the interface.

2.2 Taguchi L9 design and specimen matrix

The geometric program used a three-factor, three-level Taguchi L9 orthogonal array. The nine geometries were reproduced at each of the three nominal concrete strengths, yielding 27 unique reported observations. Geometry groups G1-G9 were retained throughout the analysis so that results at different concrete strengths but identical D, t, and L/D were treated as a physical family. The tube length was defined by L = (L/D)D. Table 2 lists the matrix. One bond-strength value was available for each grade-geometry cell; replicate-level measurements and within-cell uncertainty were not present in the source record.

Table 2
Taguchi L9 geometry matrix used at each concrete grade.

Group	D (mm)	t (mm)	L/D	L (mm)
G1	33.7	2.6	12	404.4
G2	33.7	3.2	14	471.8
G3	33.7	4.0	16	539.2
G4	42.2	2.6	14	590.8
G5	42.2	3.2	16	675.2
G6	42.2	4.0	12	506.4
G7	48.3	2.6	16	772.8
G8	48.3	3.2	12	579.6
G9	48.3	4.0	14	676.2

2.3 Push-out testing and bond-strength calculation

Push-out tests were conducted at a concrete age of 28 days using a reported 2000-ton-capacity testing machine. As illustrated in Fig. 1, the steel tube was supported while the axial load was applied directly to the concrete core through a loading block. A nominal 10 mm clearance at the lower end allowed relative displacement of the core. The source description reports an initial loading rate of 0.2 kN/s up to the onset of bond failure, followed by 2 kN/min until completion; the authors should verify this sequence against the laboratory log because the stated rate decreases after initiation. The ultimate bond stress was interpreted using the conventional uniform-interface expression

$$\tau_u = P_u / (\pi D_i L_i),$$

where L_i is the bonded interface length and P_u is the maximum push-out load. The response for all subsequent analyses was the reported τ_u values. The precise diameter convention, the length of the interface, the accuracy of the load cell, the slip-measurement set-up, and the number of replicate specimens should be established from the original laboratory records.

2.4 Statistical analysis

Pearson correlation coefficients were computed for the linear association between each pair of variables. The L9 combinations were orthogonal, and repeated across the three concrete grades, so therefore a main-effects analysis of variance (ANOVA) was executed, with the three levels of fck, D, t and L/D first presented as categorical factors. The sum of squares for each factor was obtained from the weighted deviation of the level means from the grand mean. The residual had unmodelled interactions and experimental variation. The contributions were reported as a percentage of the sum of the squares due to the factors over the sum of all the squares. The significance level of 0.05 was used. Because the design is not conducive to reliable estimation of all interactions, p values are taken as screening evidence, not as population-level inference.

2.5 Machine-learning models and leakage-resistant validation

The predictors were nominal concrete strength fck, tube diameter D, wall thickness t, and L/D; the target was ultimate bond strength τ_u. Five regression approaches were compared: ordinary linear regression, ridge regression, radial-basis-function SVR, random forest regression, and gradient boosting regression. Scaling was applied inside each training fold for linear, ridge, and SVR models. Hyperparameters were selected only from the training data using an inner four-fold GroupKFold search. The outer validation used nine GroupKFold splits defined by G1-G9: in each split, the three observations sharing one geometry were withheld together. Thus, no test geometry appeared in the corresponding training data. Predictions from all outer folds were pooled to calculate MAE, RMSE, MAPE, and R^2. This nested grouped procedure prevents the geometry leakage and model-selection optimism that can occur with random or in-sample assessment [18]. All derived analyses used fixed random seed 20260811 and standard implementations consistent with scikit-learn [19].

2.6 Taguchi, MOORA, and COPRAS optimization

Each geometry was evaluated across the three concrete grades. For Taguchi ranking, bond strength was treated as a beneficial response and the larger-the-better signal-to-noise ratio was computed as $S/N = -10 \log10[(1/n)\Sigma(1/\tau_u^2)]$. MOORA and COPRAS treated the M40, M50, and M70 bond strengths as three beneficial criteria. Entropy weights were calculated from the normalized dispersion of each grade-specific response. MOORA used vector normalization and the weighted sum of beneficial criteria. COPRAS used column-sum normalization and reported utility relative to the highest priority score. Because all responses were beneficial, no cost term was subtracted. Rank agreement across the three methods was used as evidence of a robust rather than method-specific optimum.

3. Results and discussion

3.1 Experimental bond-strength response

Across the 27 observations, τ_u ranged from 0.830 MPa (M50-G7: D = 48.3 mm, t = 2.6 mm, L/D = 16) to 2.062 MPa (M70-G9: D = 48.3 mm, t = 4.0 mm, L/D = 14). The grade-wise mean values were 1.396 MPa for M40, 1.371 MPa for M50, and 1.705 MPa for M70. The slight increase from M40 to M50 indicates that compressive strength alone was not sufficient to influence bond resistance, however, the M70 group had a significant increase in the mean. This non-monotonic intermediate response is consistent with a frictional interface where geometry, shrinkage and surface condition all play a part along with the radial contact pressure. Geometry G6 has the highest cross grade mean (1.872 MPa) and the smallest range of 1.802–1.915 MPa. The mean value for G7 was the lowest (1.015 MPa). The three favorable changes that occurred from G7 to G6 are a decrease in the L/D ratio, an increase in the wall thickness, and an intermediate diameter that will add up to the 84.4% increase in mean bond strength. The outcome should hence be considered as a multi-factors geometry effect and not to a single factor.

3.2 Main effects and ANOVA

The mean τ_u for the different t values in Fig. 2 increased with t increasing from 2.6 to 4.0 mm, with an increase of 30.4% when t was increased from 2.6 to 4.0 mm. Thicker tube is less prone to local radial deformations and is more capable of withstand larger confinement and interface pressure during push-out. In contrast, increasing L/D from 12 to 16 reduced the mean from 1.750 to 1.238 MPa, a decrease of 29.3%. A longer interface provides more time for some regions to achieve more uniform shear transfer and for separation from the interface to occur under shrinkage and for progressive debonding to occur; therefore, the average stress across the entire interface may decrease as the total load transferred increases. Diameter had a weaker, non-monotonic main effect: the means were 1.641, 1.391, and 1.440 MPa at 33.7, 42.2, and 48.3 mm, respectively. The answer is therefore NOT supporting the original draft statement that size – diameter was the most important factor. The strength of concrete was also impacted in a stepped and not entirely linear fashion, with the main improvement being at M70. These patterns are consistent with the need for an orthogonal multi-factor analysis.

Table 3
Main-effects ANOVA for ultimate bond strength.

Factor	df	SS	MS	F	p	Contribution (%)
Concrete strength	2	0.6237	0.3118	7.427	0.004	17.44
Diameter, D	2	0.3167	0.1584	3.771	0.043	8.86
Thickness, t	2	0.6947	0.3473	8.272	0.003	19.43
L/D	2	1.1844	0.5922	14.104	< 0.001	33.13
Residual	18	0.7558	0.0420	-	-	21.14
Total	26	3.5752	-	-	-	100.00

The ANOVA results quantify the visual trends. L/D made the largest contribution (33.13%, F = 14.10, p < 0.001), followed by t (19.43%, p = 0.003), concrete strength (17.44%, p = 0.004), and D (8.86%, p = 0.043).

The 21.14% residual contribution consists of interactions, experimental scatter and any effects of unreported material and surface variables. The selected factors explain 78.86% of the observed variation, which suggests that the response within the investigated domain is mainly due to the four main effects, but the residual is too large to justify deriving a design rule exclusively from a deterministic approach.

3.3 Correlation structure and linear benchmark

The orthogonal design generated almost no pairwise correlations between fck, D, t, and L/D (Fig. 3) so that the associations of their corresponding marginals with τ_u could be read without predictor collinearity. L/D showed the strongest correlation (r = -0.575), followed by t (r = 0.439), fck (r = 0.385), and D (r = -0.243). The benchmark model used was a multiple linear model that was fitted.

$$\tau_u = 2.3896 + 0.01122\,fck - 0.01479\,D + 0.27854\,t - 0.12822\,(L/D),$$

All dimensions given in MPa and mm as appropriate. The directions of the coefficients are consistent with the main-effect results. The in-sample R2 was 0.731, which is a descriptive measure and was not a predictive measure as the model was fitted with the in-sample observations. Next, the performance data are grouped out-of-sample.

3.4 Machine-learning generalization

Table 4
Performance under nested geometry-grouped cross-validation.

Model	MAE (MPa)	RMSE (MPa)	MAPE (%)	R^2
Support vector regression	0.157	0.193	10.87	0.719
Ridge regression	0.187	0.212	13.19	0.661
Linear regression	0.189	0.215	13.31	0.652
Gradient boosting	0.265	0.301	20.32	0.317
Random forest	0.296	0.341	22.33	0.124

SVR was the best model under the leakage-resistant assessment, with R^2 = 0.719, RMSE = 0.193 MPa, MAE = 0.157 MPa, and MAPE = 10.87%. The dominant response is relatively smooth, low-dimensional, and was followed by ridge and ordinary linear regression (R 2 = 0.661 and 0.652), respectively. Gradient boosting and random forest took a huge hit with R^2 values of 0.317 and 0.124 respectively. As predicted, they compressed their test predictions towards the training mean when they were required to extrapolate to a combination of geometries not present in the training. This ranking is a change from the original draft, where apparent fit metrics were used, and the original draft conclusion was that Random Forest's R^2 was approximately 0.91. The difference is not cosmetic, but methodologic: Original model predictions closely matched the data for the models that were developed, while the present test requires the model to predict an unseen geometry. Grouped result is more representative estimation of generalization for

structured dataset with 27 observations. Deep neural networks and convolutional neural networks were therefore not considered; they require much larger external databases to be parameterized in a way that is defensible with this sample size and tabular input. The value obtained from the SVR is encouraging, but should be applied only for interpolation in the range of the tested values.

3.5 Multi-criteria optimization

Table 5
Cross-grade performance and optimization ranks.

Geometry	D (mm)	t (mm)	L/D	Mean τ_u (MPa)	Taguchi	MOORA	COPRAS
G1	33.7	2.6	12	1.713	3	4	4
G2	33.7	3.2	14	1.662	2	2	2
G3	33.7	4.0	16	1.549	6	6	6
G4	42.2	2.6	14	1.152	7	7	7
G5	42.2	3.2	16	1.149	8	8	8
G6	42.2	4.0	12	1.872	1	1	1
G7	48.3	2.6	16	1.015	9	9	9
G8	48.3	3.2	12	1.667	4	3	3
G9	48.3	4.0	14	1.637	5	5	5

The entropy weights assigned to the M40, M50, and M70 responses were 0.4168, 0.4638, and 0.1194, respectively. The numbers reflect the ability of the grade level geometry-specific responses to discriminate among the geometry, not the importance of the grades in the physical world. The largest S/N ratio (5.437 dB), MOORA score (0.4329), and COPRAS utility (1.000) were obtained by G6. It also had the highest mean score of 1.872 MPa across grades. The three grade-specific values were within 0.113 MPa of each other, indicating that the chosen geometry was not only highly resistant to grade, but also highly resistant. In a positive data set, the orderings resulting from the normalizations of MOORA and COPRAS were the same since all three criteria are desirable and employed the same entropy weights. Taguchi was able to agree to the best and worst geometries, although he switched some of the intermediate values due to the greater penalties incurred by the low values by the larger-the-better S/N ratio. The order of the first rank of G6 is therefore well preserved with both the decision rules. The worst geometry was G7 (D = 48.3 mm, t = 2.6 mm, L/D = 16), with mean τ_u = 1.015 MPa, MOORA score 0.2058, and COPRAS utility 0.4747.

3.6 Engineering implications and limitations

As far as the range investigated is concerned, the geometry which is most reliable to improve interfacial resistance is to reduce L/D and increase wall thickness. This leads to physically consistent shorter transfer length, slower debonding progression, and greater radial restraint. The strength of concrete is

useful primarily at the M70 level; the diameter should not be considered a monotonic design variable. The optimum is an observed, not a mathematically-derived one, and should not be extrapolated outside of the ranges of D = 33.7–48.3 mm, t = 2.6-4.0 mm, L/D = 12–16, or fck = 40–70 MPa. There are a few restrictions that limit the next experimental step. First of all, there is no data available at a replicate level, which means that repeatability and confidence intervals cannot be quantified. Secondly, no load-slip curves, local strain measurements, failure photographs, steel properties, galvanizing thickness, surface roughness or shrinkage information is provided as part of this record. Thirdly, the lack of an ungalvanized control does not allow for separating the coating effect from the geometry. Fourth, 27 observations are enough to be screened, but not enough to be used for a general ML design model. A more rigorous validation program should repeat the L9 cells, incorporate control surface conditions, quantify the complete bond-slip response, and evaluate an external geometry set, not developed with the model.

4. Conclusions

1. The 27 reported push-out observations produced ultimate interfacial bond strengths from 0.830 to 2.062 MPa. Geometry G6 (D = 42.2 mm, t = 4.0 mm, L/D = 12) delivered the highest and most stable cross-grade response: 1.899, 1.915, and 1.802 MPa for M40, M50, and M70, respectively.
2. L/D was the dominant main effect, contributing 33.13% of the total variation. Wall thickness (19.43%) and concrete strength (17.44%) were also significant, while diameter had a smaller and non-monotonic contribution (8.86%).
3. Increasing wall thickness from 2.6 to 4.0 mm increased the mean bond strength by 30.4%, whereas increasing L/D from 12 to 16 reduced it by 29.3%. These trends support the use of short, thick-walled geometries when interfacial transfer is critical.
4. Under nested geometry-grouped validation, SVR generalized best (R^2 = 0.719, RMSE = 0.193 MPa, MAPE = 10.87%). Random Forest did not retain the high performance suggested by in-sample fitting, demonstrating the importance of leakage-resistant validation for compact orthogonal designs.
5. Taguchi, entropy-weighted MOORA, and COPRAS unanimously ranked G6 first. Agreement among the methods confirms that its selection is not an artifact of a single normalization or decision rule.
6. The findings are applicable only within the tested ranges and cannot isolate the effect of galvanizing. Replicated push-out tests, complete bond-slip curves, steel/coating characterization, and independent external validation are required before developing a general design equation.

Declarations

Funding Information:

This research received no specific grant from any funding agency in the public, commercial, or not-for-profit sectors.

Author Contribution

Chethan Kumar S: Conceptualization, Methodology, Writing – Original Draft. Sandesh N U: Data Curation, Formal Analysis. Anusha T S: Software, Writing – Review & Editing. N S Kumar: Review and Editing. Syed Sharfuddin: Formal Analysis, Data Curation. Apsar Pasha: Conceptualization, Review and Editing. All authors have read and agreed to the published version of the manuscript.

Acknowledgement

Nil

References

1. Roeder CW, Cameron B, Brown CB. Composite action in concrete filled tubes. Journal of Structural Engineering. 1999;125(5):477–484. https://doi.org/10.1061/(ASCE)0733-9445(1999)125:5(477).
2. Tao Z, Song TY, Uy B, Han LH. Bond behavior in concrete-filled steel tubes. Journal of Constructional Steel Research. 2016;120:81–93. https://doi.org/10.1016/j.jcsr.2015.12.030.
3. Shakir-Khalil H. Pushout strength of concrete-filled steel hollow section tubes. The Structural Engineer. 1993;71(13):230–243.
4. Qu X, Chen Z, Nethercot DA, Gardner L, Theofanous M. Load-reversed push-out tests on rectangular CFST columns. Journal of Constructional Steel Research. 2013;81:35–43. https://doi.org/10.1016/j.jcsr.2012.11.003.
5. Xu C, Chengkui H, Decheng J, Yuancheng S. Push-out test of pre-stressing concrete filled circular steel tube columns by means of expansive cement. Construction and Building Materials. 2009;23(1):491–497. https://doi.org/10.1016/j.conbuildmat.2007.10.021.
6. Tao Z, Han LH, Uy B, Chen X. Post-fire bond between the steel tube and concrete in concrete-filled steel tubular columns. Journal of Constructional Steel Research. 2011;67(3):484–496. https://doi.org/10.1016/j.jcsr.2010.09.006.
7. Song TY, Tao Z, Han LH, Uy B. Bond behavior of concrete-filled steel tubes at elevated temperatures. Journal of Structural Engineering. 2017;143(11):04017147. https://doi.org/10.1061/(ASCE)ST.1943-541X.0001890.
8. Lyu WQ, Han LH. Investigation on bond strength between recycled aggregate concrete and steel tube in RAC-filled steel tubes. Journal of Constructional Steel Research. 2019;155:438–459. https://doi.org/10.1016/j.jcsr.2018.12.028.
9. Dong H, Chen X, Cao W, Zhao Y. Bond-slip behavior of large high-strength concrete-filled circular steel tubes with different constructions. Journal of Constructional Steel Research. 2020;167:105951. https://doi.org/10.1016/j.jcsr.2020.105951.

10. Dai P, Yang L, Wang J, Fan J, Lin M. Experimental study on the steel-concrete bond behaviour of circular concrete-filled stainless steel tubes. Thin-Walled Structures. 2021;169:108506. https://doi.org/10.1016/j.tws.2021.108506.
11. Liu Z, Lu Y, Li S, Xiao L. Enhanced bond-slip behavior between recycled aggregate concrete and steel tubes under repeated loading. Structures. 2021;33:1263–1282. https://doi.org/10.1016/j.istruc.2021.05.022.
12. Taguchi G. Introduction to Quality Engineering: Designing Quality into Products and Processes. Tokyo: Asian Productivity Organization; 1986.
13. Brauers WKM, Zavadskas EK. The MOORA method and its application to privatization in a transition economy. Control and Cybernetics. 2006;35(2):445–469.
14. Shannon CE. A mathematical theory of communication. Bell System Technical Journal. 1948;27:379–423, 623–656. https://doi.org/10.1002/j.1538-7305.1948.tb01338.x.
15. Almasaeid HH, Salman DG, Abendeh RM, Allouzi RA, Rabayah HS. Interfacial bond capacity prediction of concrete-filled steel tubes utilizing artificial neural network. Cogent Engineering. 2024;11(1):2297501. https://doi.org/10.1080/23311916.2023.2297501.
16. Allouzi RA, Almasaeid HH, Salman DG, Abendeh RM. Prediction of bond-slip behavior of circular/squared concrete-filled steel tubes. Buildings. 2022;12(4):456. https://doi.org/10.3390/buildings12040456.
17. Breiman L. Random forests. Machine Learning. 2001;45:5–32. https://doi.org/10.1023/A:1010933404324.
18. Varma S, Simon R. Bias in error estimation when using cross-validation for model selection. BMC Bioinformatics. 2006;7:91. https://doi.org/10.1186/1471-2105-7-91.
19. Pedregosa F, Varoquaux G, Gramfort A, et al. Scikit-learn: Machine learning in Python. Journal of Machine Learning Research. 2011;12:2825–2830.
20. Cortes C, Vapnik V. Support-vector networks. Machine Learning. 1995;20:273–297. https://doi.org/10.1007/BF00994018.
21. Friedman JH. Greedy function approximation: A gradient boosting machine. The Annals of Statistics. 2001;29(5):1189–1232. https://doi.org/10.1214/aos/1013203451.
22. Bureau of Indian Standards. IS 10262:2009. Concrete Mix Proportioning-Guidelines. New Delhi: BIS; 2009.
23. Bureau of Indian Standards. IS 516. Methods of Tests for Strength of Concrete. New Delhi: BIS.

Appendix

Appendix A. Experimental dataset

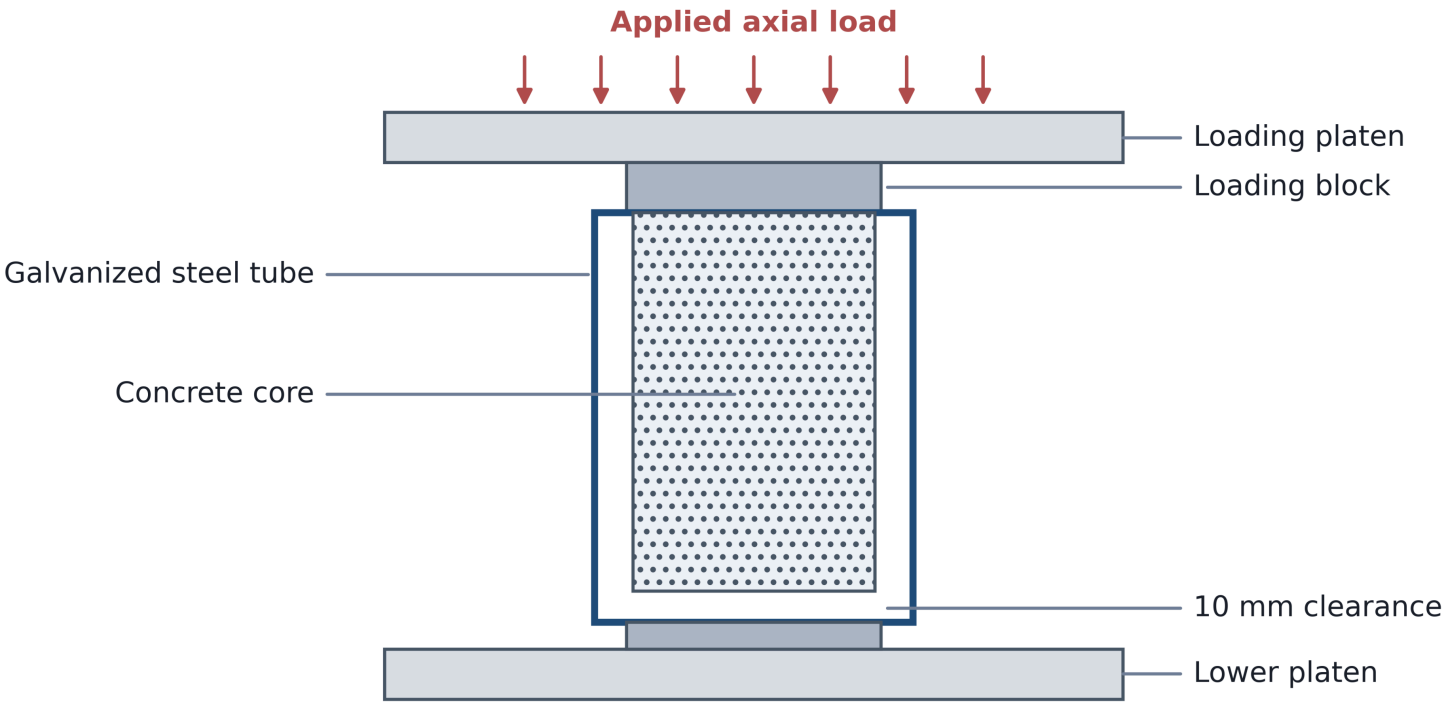
Table A1 reproduces the 27 reported bond-strength observations used in every derived analysis. Values are preserved from the source results table; no experimental response has been invented or imputed.

Table A1
Verified experimental dataset.

Specimen	fck (MPa)	D (mm)	t (mm)	L/D	τ_u (MPa)
C40-G1	40	33.7	2.6	12	1.770
C40-G2	40	33.7	3.2	14	1.541
C40-G3	40	33.7	4.0	16	1.558
C40-G4	40	42.2	2.6	14	0.991
C40-G5	40	42.2	3.2	16	0.923
C40-G6	40	42.2	4.0	12	1.899
C40-G7	40	48.3	2.6	16	0.878
C40-G8	40	48.3	3.2	12	1.372
C40-G9	40	48.3	4.0	14	1.631
C50-G1	50	33.7	2.6	12	1.360
C50-G2	50	33.7	3.2	14	1.781
C50-G3	50	33.7	4.0	16	1.282
C50-G4	50	42.2	2.6	14	1.083
C50-G5	50	42.2	3.2	16	0.979
C50-G6	50	42.2	4.0	12	1.915
C50-G7	50	48.3	2.6	16	0.830
C50-G8	50	48.3	3.2	12	1.888
C50-G9	50	48.3	4.0	14	1.219
C70-G1	70	33.7	2.6	12	2.008
C70-G2	70	33.7	3.2	14	1.664
C70-G3	70	33.7	4.0	16	1.806
C70-G4	70	42.2	2.6	14	1.381
C70-G5	70	42.2	3.2	16	1.545
C70-G6	70	42.2	4.0	12	1.802
C70-G7	70	48.3	2.6	16	1.337
C70-G8	70	48.3	3.2	12	1.740

Specimen	fck (MPa)	D (mm)	t (mm)	L/D	τ_u (MPa)
C70-G9	70	48.3	4.0	14	2.062

Figures



Load is applied to the concrete core while the steel tube is supported

Figure 1

Schematic of the push-out loading principle used to mobilize relative slip between the concrete core and galvanized steel tube. The drawing has been redrafted from the experimental schematic supplied with the source manuscript.

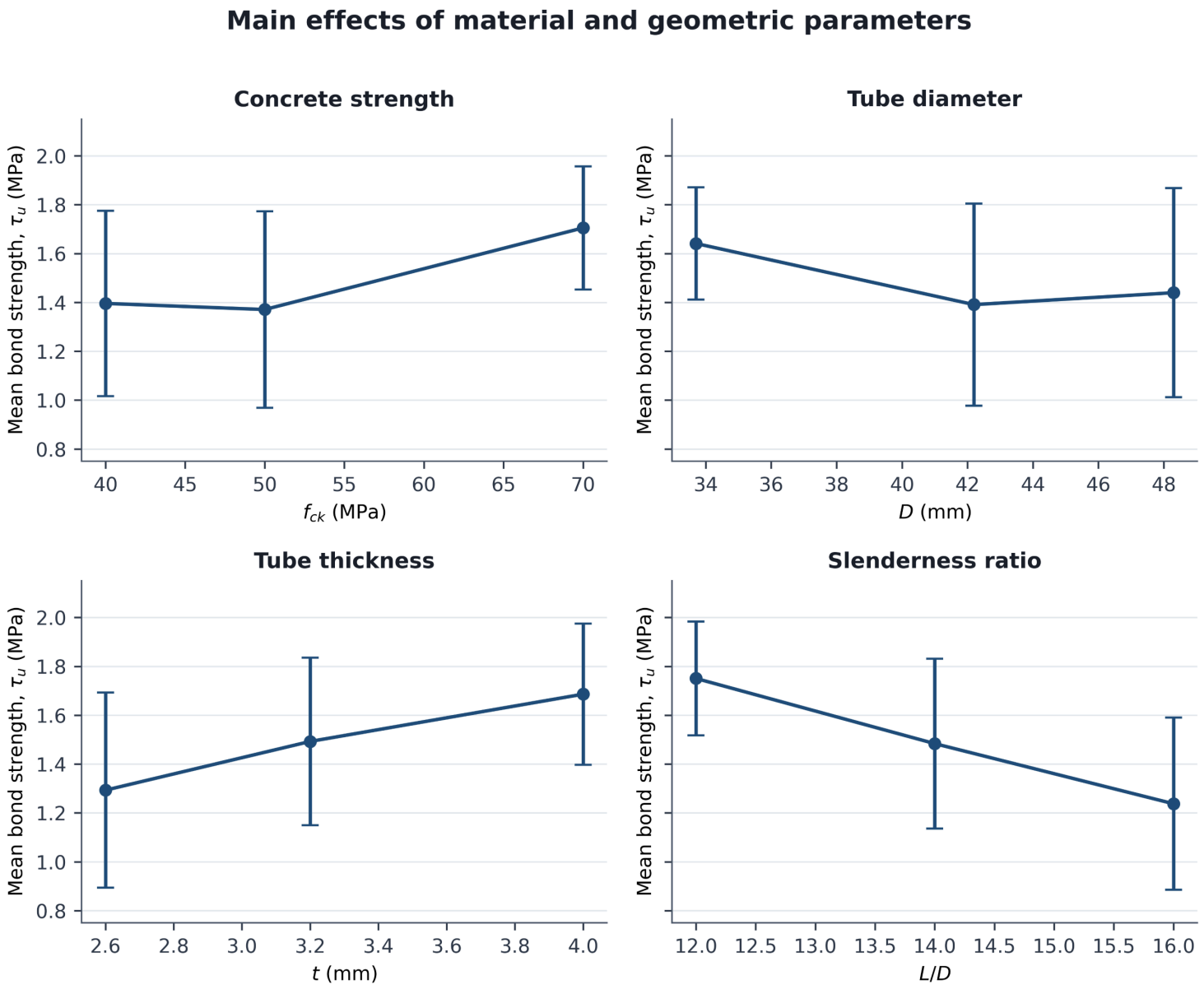


Figure 2

Main effects for ultimate bond strength for nominal concrete strength, tube diameter, wall thickness and L/D ratio. Level means are indicated by markers and error bars represent the standard deviation of the nine observations for each level.

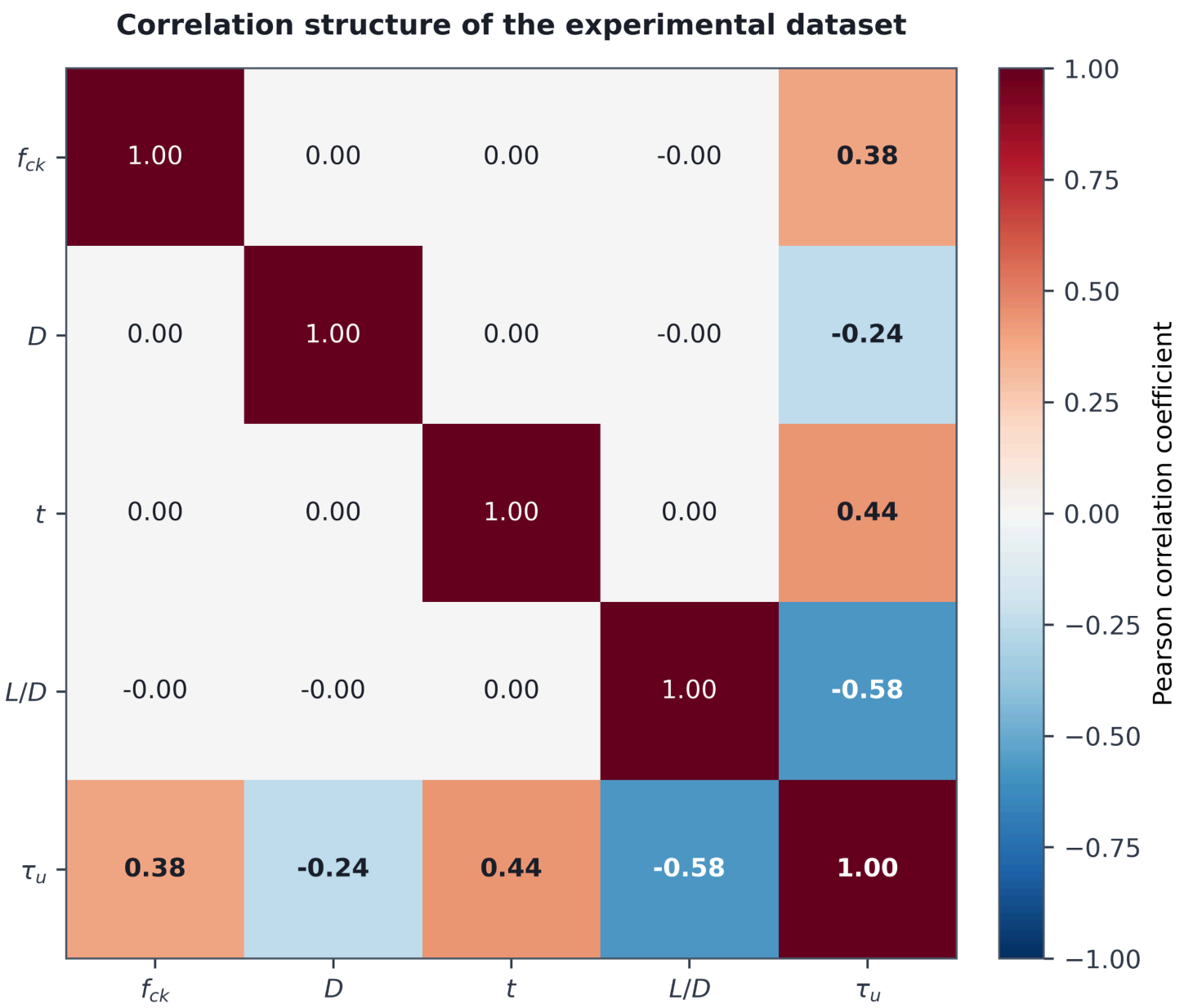


Figure 3

Pearson correlation matrix for the four predictors and measured ultimate bond strength. Orthogonality of the L9 design is reflected by near-zero correlations among geometric predictors.

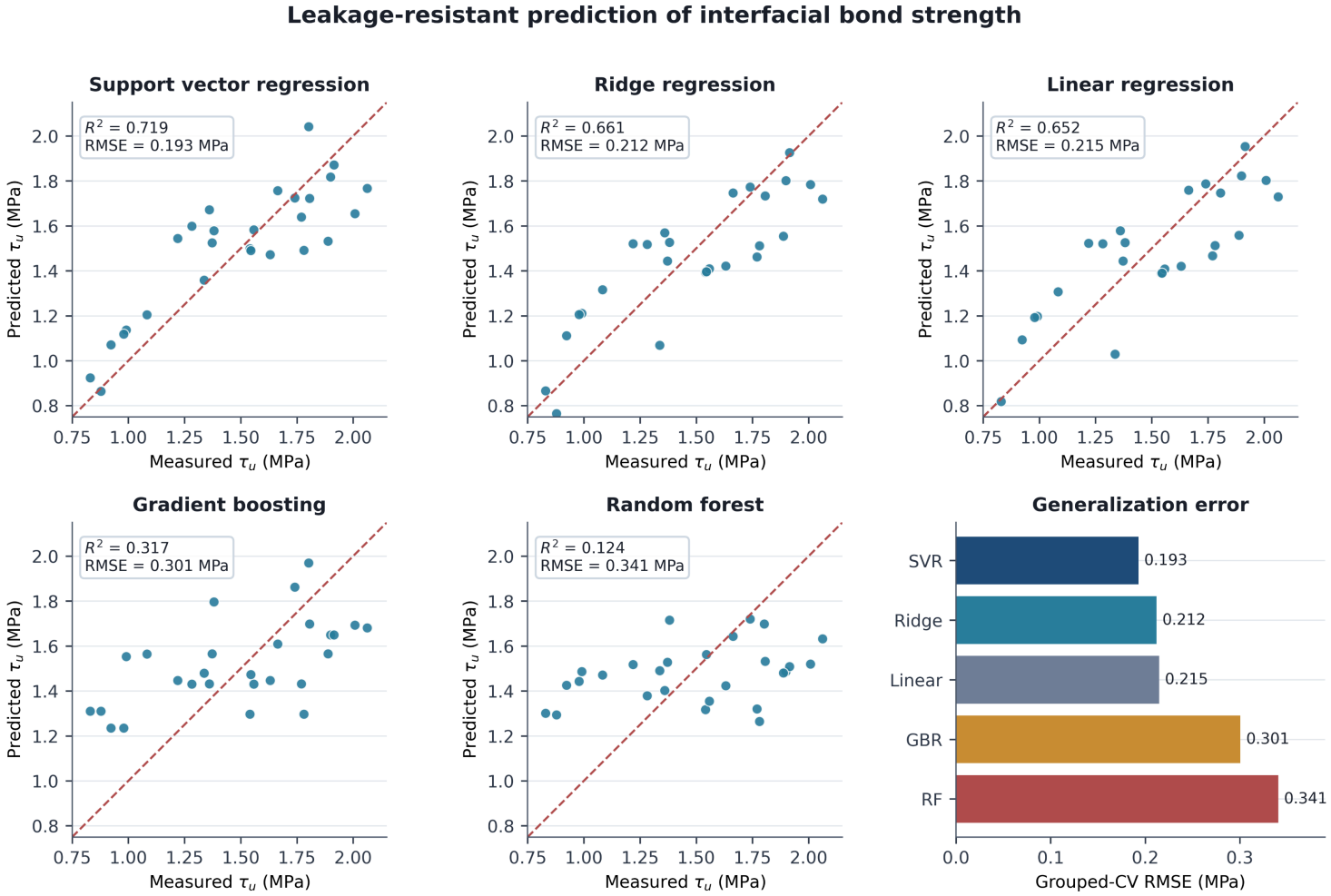


Figure 4

Measured versus predicted bond strength from nested geometry-grouped cross-validation. Each outer fold withheld all three concrete grades associated with one L9 geometry. The dashed line denotes perfect agreement.

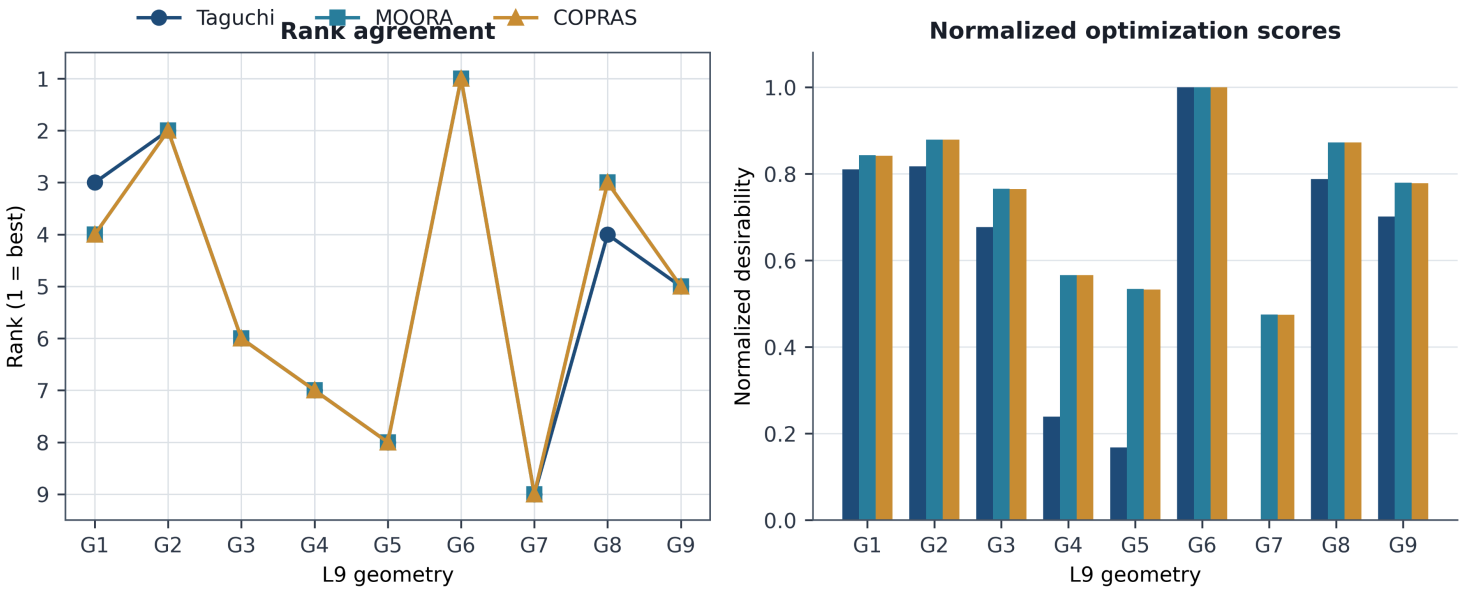


Figure 5

Comparison of Taguchi larger-the-better, entropy-weighted MOORA, and COPRAS results. All three methods identify G6 (D = 42.2 mm, t = 4.0 mm, L/D = 12) as the preferred geometry.